Reference: *Biol. Bull.* **188:** 8–15. (February/March, 1995)

Inorganic Overgrowth of Aragonite on Molluscan Nacre Examined by Atomic Force Microscopy

R. GILES[1,*], S. MANNE[1], S. MANN[2], D. E. MORSE[3], G. D. STUCKY[4], AND P. K. HANSMA[1,†]

[1]*Department of Physics, University of California, Santa Barbara, California 93106,*
[2]*School of Chemistry, University of Bath, Claverton Down, Bath BA2 7AY, United Kingdom,*
[3]*Marine Biotechnology Center, Marine Science Institute, University of California, Santa Barbara, California 93106, and* [4]*Department of Chemistry, University of California, Santa Barbara, California 93106*

Abstract. The nacre (mother-of-pearl) that forms the iridescent inner layers of mollusc shells is a highly ordered microlaminate composite of aragonite crystals and biopolymers with a strength and fracture resistance that far exceed those of the mineral crystals themselves. The processes governing the biofabrication of this material by the secretory cells of the mantle are complex and only partially understood. We have used the atomic force microscope (AFM) to investigate the aqueous solution conditions under which mineral growth can occur on the nacreous layer of the shell of the bivalve mollusc *Atrina* sp. *In situ* imaging of the mature nacre surface exposed to a pH-controlled environment of natural seawater with added carbonate ions reveals that inorganic overgrowth of aragonite can occur within the ranges of pH and inorganic ion concentrations found in the molluscan extrapallial fluid from which the mineral is produced during biological shell growth. Thus, we posit that once nucleation has occurred, nacreous tablets could grow inorganically in the extrapallial space; the role of proteins and other macromolecules may be limited to initiating growth or controlling morphology through selective adsorption and spatial constraint on the growing crystal.

Introduction

The mineral shells of a variety of molluscs are composite biomaterials consisting of crystals of calcium carbonate ($CaCO_3$) intercalated with organic materials, primarily proteins and glycoproteins (reviewed in Wilbur, 1972; Towe, 1972; Watabe, 1981; Weiner, 1986; Simkiss and Wilbur, 1989; Lowenstam and Weiner, 1989). The $CaCO_3$ occurs in two predominate crystal phases within shells: calcite and aragonite. A shell may contain one phase or the other, or both, depending on the animal species, but commonly the stronger, denser aragonite forms an inner structural layer, while calcite forms the outer layer. The inner structural layer, called nacre or mother-of-pearl, is a complex microlaminate composed of polygonal "tablets" of aragonite that measure 5 to 15 μm across, but only 0.5 to 1 μm in thickness, packed together with a thin (40 nm) "mortar" of organic macromolecules. The organic component thus amounts to a small portion of the total shell: less than 10% (Addadi and Weiner, 1992). It nevertheless is responsible for the excellent strength and resistance to crack propagation of the molluscan shell. Crystallographically, the *a* and *b* axes lie in the plane of the aragonitic tablets, with the *c* axis uniformly perpendicular to the surface.

The nacreous layer of molluscan shell has been studied extensively for several decades, principally with x-ray and electron microscopic techniques. This work has been largely successful in describing the microstructure of nacre (see Lowenstam and Weiner, 1989; Weiner, 1986; Watabe, 1981; Towe, 1972; and Wise, 1970, for reviews). Various calcium-binding, highly acidic, water-soluble proteins have been isolated from the shell in various developmental stages (Cariolou and Morse, 1988). Water-insoluble proteins from the shell have been characterized

Received 7 March 1994; accepted 4 November 1994.

* Present address: Department of Physics, Simon Fraser University, Burnaby, British Columbia, Canada V5A 1S6.

† Author to whom correspondence should be addressed.

with x-ray diffraction, leading to the conclusion that they resemble silk fibroin (Weiner and Traub, 1980). Both the water-soluble and the water-insoluble proteins have been proposed as multilaminar templates for the mineral tablets (Nakahara *et al.*, 1982).

The mechanism of growth of the nacreous layer is complex and not well understood. It is known that both organic and inorganic components are secreted by epithelial cells in the mantle tissue into the extrapallial space (the extracellular cavity between the mantle and the shell, which is sealed from the surrounding environment), bathing the growing shell in a mixture called the extrapallial fluid. Although the inorganic components of the extrapallial fluid are obviously necessary for mineral growth, it is not known whether they are sufficient: *i.e.*, the role of the organic components is not well known. Kitano and Hood (1962) showed that aragonite is the most favorable phase of $CaCO_3$ to nucleate in seawater supersaturated with respect to that mineral; the presence of Mg^{2+} in solution apparently acts to select aragonite over calcite. Others have measured nucleation rates of aragonite crystals in seawater and artificial extrapallial fluid (Pytkowicz, 1965; Wilbur and Bernhardt, 1984). We extended these studies by making two experimental modifications relevant to nacreous growth. First, we studied crystallization directly on a nacreous surface (rather than unseeded nucleation in solution). (Recently, Sabbides and Koutsoukos [1993] also investigated seeded growth of aragonite on a variety of substrates in seawater.) Second, we controlled both pH and total carbonate concentration simultaneously, and we compare growth conditions to those values reported for extrapallial fluid.

We have used the atomic force microscope (AFM) (Binnig *et al.*, 1986) to examine the conditions for inorganic growth of the nacre tablets. (For reviews of the AFM, see Rugar and Hansma, 1990; Sarid, 1991; Hoh and Hansma, 1992). The AFM (also known as the scanning force microscope) is a member of the family of scanning probe microscopes; these instruments form images by raster scanning a tiny probe over the surface of the sample while mapping some local interaction, such as electron tunneling or near-field optical effects, as a function of position. The AFM probe consists of a flexible cantilever, $\sim 100\ \mu m$ long, with a sharp tip attached at the end; the probe measures (through the elastic response of the cantilever) the interaction forces between the tip and the sample. The probe can thus map surface topography by scanning in gentle contact with the sample; the displacement of the cantilever (as the tip slides over surface features) is detected from the motion of a laser beam reflected from the back of the cantilever onto a position-sensing photodiode. The AFM can operate in solution and hence allows *in situ* imaging of samples from the micrometer to the nanometer scale. It recently has been applied to biomineralized composites such as diatom shells (Linder *et al.*, 1992), bone (Tao and Lindsay, 1992), teeth (Kasas *et al.*, 1993), pressed powders of clam shells and sea urchin shells (Friedbacher *et al.*, 1991), and molluscan nacre (Manne *et al.*, 1994). It has imaged *in situ* dynamic processes on relevant systems such as calcite (Gratz *et al.*, 1993; Hillner *et al.*, 1992), fluorite (Hillner *et al.*, 1993), and hydroxyapatite (Kasas *et al.*, 1993), as well as calcite growth modification in the presence of polyamino acids (Wierzbicki *et al.*, 1993) and inorganic poisons (Gratz and Hillner, 1993; Dove and Hochella, 1993). By examining the exposed aragonite surface of mature nacreous tablets for signs of growth under various solutions, we bracketed and thus defined the conditions under which aragonite growth can occur. These conditions are biologically relevant: the solutions used approximate the inorganic components of the extrapallial fluid in which new nacre is formed.

Materials and Methods

Samples of nacre from the bivalve *Atrina* sp. were kindly provided by Prof. S. Weiner at the Weizmann Institute of Science in Israel. For imaging, small pieces (approx. $1 \times 0.5 \times 0.1$ mm) of mature nacre were prepared by mechanically cleaving a shell fragment with a razor blade and then fracturing the resulting chip down to the desired dimensions.

The solutions tested were based on natural seawater collected locally from the Pacific Ocean along the Santa Barbara coast. The water was coarsely filtered, irradiated with ultraviolet light, passed through a 0.2-μm filter, and stored at 2°–4°C in a sterilized, lightproof container until just before use. To the seawater various amounts of $NaHCO_3$ were added, and the pH was adjusted to the desired value by addition of HCl or NaOH.

Cation concentrations for the filtered seawater were measured by atomic absorption spectroscopy; total carbonate ion concentration was determined by titration with HCl. Table 1 lists concentrations for the measured ions (at about 20°C). These agree well with previously published concentrations for seawater (Crenshaw, 1972; Smith, 1974; Wada and Fujinuki, 1976). In addition, the cation concentrations are all within about 10% of the published values for the extrapallial fluid of bivalves. In particular, the concentration of Ca^{2+} ion we determined (Table 1) is about the same as found in extrapallial fluid (Crenshaw, 1972; Wada and Fujinuki, 1976). The major difference between seawater and the inorganic composition of extrapallial fluid is the higher concentration of carbonate ion, which is approximately

Table I

Concentrations of inorganic ions in the filtered natural seawater

Ion	Concentration (m*M*) ± standard dev.
Na^+	463 ± 2
K^+	10.9 ± 0.9
Mg^{2+}	63.1 ± 1.4
Ca^{2+}	10.3 ± 0.1
Sr^+	0.085 ± 0.007
HCO_3^- + CO_3^{2-} or total carbonate	2.3 ± 0.1

2-fold higher in extrapallial fluid. Therefore, only carbonate ion was added to natural seawater to create the growth solutions. A comparison of the values of ion concentrations determined for seawater and extrapallial fluid is included in Figure 5.

The samples of nacre were glued to a stainless steel disk with epikot resin and placed in the fluid cell of a commercial AFM (Nanoscope III from Digital Instruments, Santa Barbara, CA 93103). Samples were always oriented with the proximal side (the side facing the animal during life) exposed for imaging. After an appropriate area had been selected by imaging in air, growth solution was added to the fluid cell. The sample was examined for signs of growth for 15–20 min under a steady gravity flow of this solution. Typical flow rates were 5 μl/s, which corresponds to a replacement of the fluid cell volume every few seconds. The tip was then withdrawn and flow stopped for 1.5 h to allow more time for growth to occur. Only the exit line was blocked so that the cell remained in chemical contact with at least 40 ml of the solution in a reservoir above the cell. The sample was then examined again under flow for signs of growth. The procedure was repeated with an alternate growth solution; either the pH was raised while maintaining the same carbonate concentration, or *vice versa*. After growth had occurred with a given solution, only one or two more solutions could be tried with a given sample before the surface became so rough that further growth could not be analyzed. All growth experiments were conducted at about 20°C.

Results

Figure 1 shows an AFM image of the nacreous surface. Most of one polygonal tablet and portions of two others can be seen. The characteristic features of bivalve nacre (Manne *et al.*, 1994), such as concavity of the proximal tablet surfaces, a depression in the center of each of tablet, and elongate rings surrounding the depressions, are visible. Growth assessment was somewhat difficult at this scale; usually the characterization was made on the basis of images only 3-μm square, such as the area outlined in the figure.

Figure 2 illustrates the changes in surface roughness considered indicative of growth. It shows the same area (the inset in Fig. 1) before and after incubation for 1.5 h in seawater with a total carbonate concentration of 4.3 m*M*. In the sample imaged in Figure 2a, the pH was 7.9, at which point the surface had already changed somewhat from its initial appearance under plain seawater. The sample then was incubated for 1.5 h in a solution with the same total carbonate concentration, but at pH 8.1, and then shifted once more to pH 8.3. In Figure 2b the surface is shown 6 min after raising the pH to 8.3; further growth had occurred. As the images are shaded proportionally to height, the new growth can be seen by comparing the relative brightness of corresponding features in the two images; a few prominent pairs are indicated by arrows.

It is important to recognize that tip convolution (Grütter *et al.*, 1992; Allen *et al.*, 1992) dominates the growth image. This is indicated by the similarity of shape and orientation among the bumps on the surface.

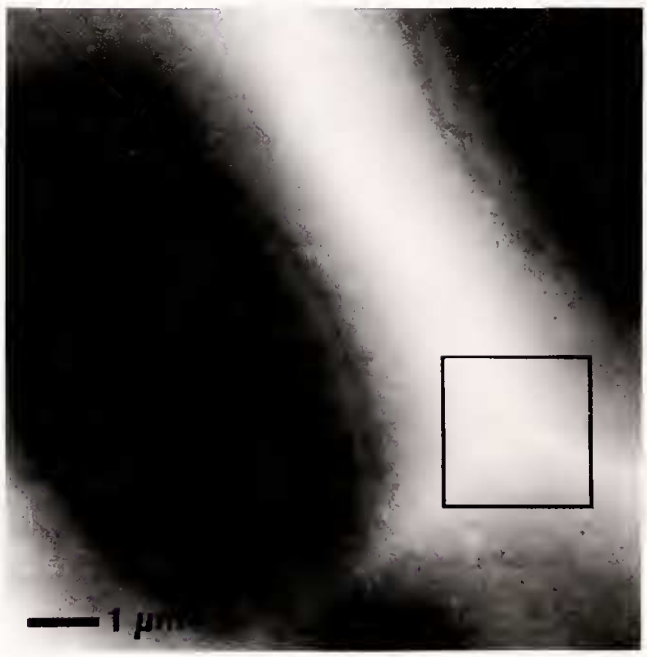

Figure 1. Atomic force microscope (AFM) image of the nacre of *Atrina* sp. The image is 11 μm^2. Shading is proportional to elevation, 500 nm from dark to light, with the brightest regions being the highest. The high ridge coincides with the boundary between nacreous tablets. Most of a tablet is visible in the center and left of the image, along with portions of two others. Note the general concavity, central depression and the elongate rings characteristic of bivalve nacre. The black square marks the area shown in Figure 2, centered on the intersection of the three tablet boundaries.

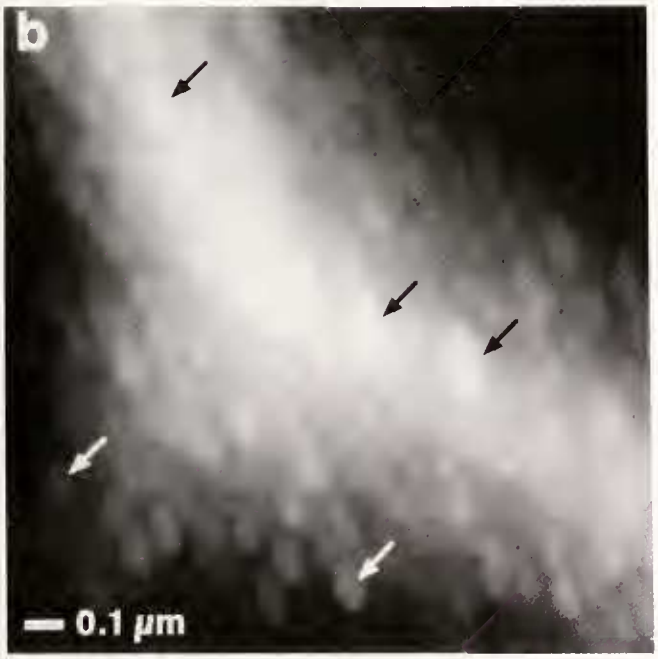

Figure 2. AFM images of the area indicated in Figure 1 before and after mineral overgrowth. Both images are 2.5 μm square; the height is 200 nm from dark to white. Comparison of corresponding features between (a) (before overgrowth) and (b) (after overgrowth) demonstrates the characteristic increase in the height of the surface asperities indicative of mineral growth on the nacreous surface. Details in text. Arrows indicate corresponding prominent asperities in the two images. These images demonstrate the topographic changes used to characterize specific solution conditions as productive of mineral overgrowth (Fig. 5).

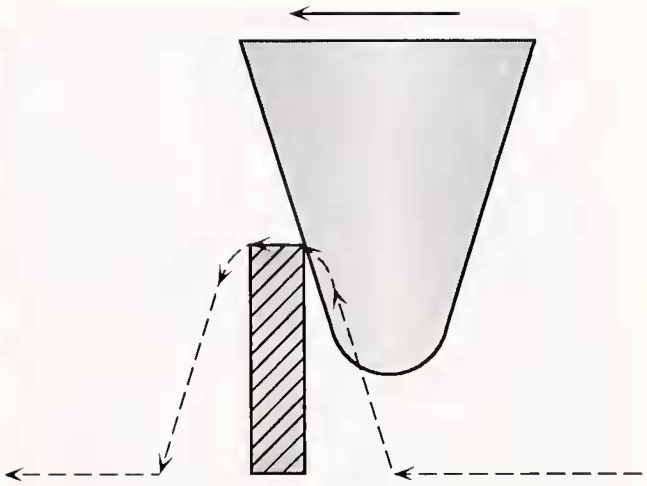

Figure 3. Illustration of the convolution between the AFM tip and a sharp asperity on the sample surface as it is scanned. The tip is shown passing from right to left over the asperity. The measured topography (dashed line) is a "convolution" of the tip shape and the asperity; it is largely an image of the tip itself, except at the very top of the asperity. Note that while the true width of the asperity is completely obscured, the height measurement is accurate.

Tip convolution is a common AFM imaging artifact; Figure 3 illustrates the mechanism responsible for this effect. The AFM measures topography by scanning a tip over the surface and measuring the vertical deflection of that tip as it slides over surface features. However, as the tip slides over an asperity with a higher aspect ratio than the tip itself, the deflection of the tip traces the tip's profile, rather than that of the asperity. In Figure 3, the dashed line indicates the path that will be traced by the tip as it passes over an asperity. Although as a consequence of tip convolution the lateral dimensions of a sharp asperity are not resolved, the overall height of that asperity is correctly measured, as is topography on the flat top (Grütter *et al.*, 1992; Allen *et al.*, 1992); thus, reliance on changes in local height detected by the AFM is justified as a measure of mineral growth. Figure 2b is consistent with the observation of surface asperities lengthening normal to the imaging plane, as expected for aragonite needles growing in their normal crystallographic habit along the *c* axis.

Although our classification of specific solution conditions into growth/no-growth categories was based on qualitative comparison of surface topography between "before" and "after" images (of which the images in Fig. 2 are an example), this method is further supported by quantitative measurements of surface roughness. Measurements of the root-mean-square deviation of height values from their collective mean was made for corresponding areas of the images in Figure 2, as well as for

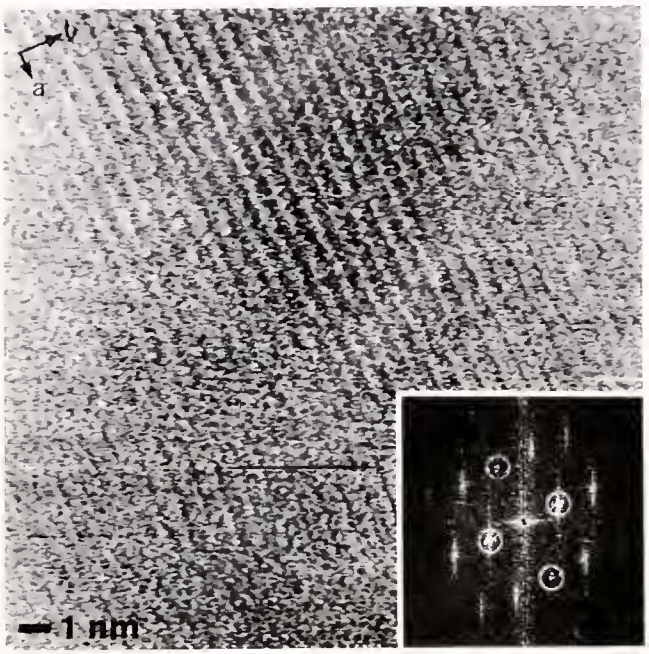

Figure 4. Unfiltered AFM image of the aragonite lattice, viewed along the *c* axis to show the (001) crystallographic plane, 30 nm square. The image was obtained on an area where overgrowth had been observed. The inset shows a Fourier transform of the image. All peaks in the transform are consistent with the expected reciprocal lattice of aragonite, and the fundamental translation vectors (circled) that define the unit cell agree with the aragonite *a* and *b* axis spacing (0.495 nm and 0.796 nm, respectively) to within 5%.

one intermediate between the two (at pH 8.1). Combining such measurements from two different areas, both away from the high tablet boundary in the center of the image, yielded a monotonically increasing surface roughness (of 2.9 nm for Fig. 2a, 3.9 nm for Fig. 2b, and 3.4 nm for the intermediate image) in agreement with the qualitative assessment of growth.

The observed changes in topography of the nacreous tablets we imaged were caused by crystal growth on the tablet surfaces, rather than by *de novo* nucleation and precipitation from the growth solution. Parallel growth experiments performed on nacreous particles embedded in epoxy showed changes in surface roughness (growth of crystal asperities) only on the nacre, and not on the surrounding epoxy. These results are described in detail elsewhere (Giles *et al.*, 1993).

Atomic lattice resolution could sometimes be obtained atop the asperities, indicating that they are terminated by small (<50 nm) flat areas. However, a wide variety of lattices were observed, perhaps indicating the presence of high-index planes on the sidewalls of the asperities. Occasionally lattices (Fig. 4) did show periodicities corresponding to the expected unit cell of the (001) plane of aragonite (*i.e.*, viewed along the *c* axis).

Figure 5 presents a summary of the growth results. The dashed lines separate the values of total carbonate concentration and pH that define the growth and no-growth conditions. The rectangular bands designate the ranges of these values previously reported for molluscan extrapallial fluid and natural seawater. Note that growth never occurs at the carbonate concentrations of seawater, but that the boundary between growth and no-growth cuts across the extrapallial fluid range, suggesting the potential for dynamic control of shell formation by changes in extrapallial fluid composition. This is consistent with previous data on seasonal variation in the acidity of the extrapallial fluid, in which high pH was correlated with a high rate of shell growth and low pH with slow growth or shell dissolution (Wada, 1961).

Supersaturation values of specific ions with respect to aragonite were estimated with the IONPRODUCT computer program (Shellis, 1988) for each of the solutions tested. Saturation fractions ranged from 0.3 to 3.6, but in general (with two exceptions) overgrowth occurred at saturation values greater than 1, and no overgrowth occurred at saturation values less than 1.

Discussion

The nacre of molluscan shell is a highly organized microlaminate composite of proteins, glycoproteins, and calcium carbonate crystals in the aragonite phase; the

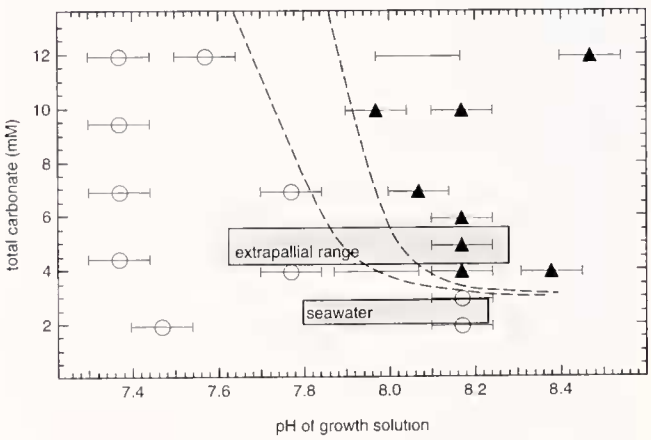

Figure 5. Aragonite growth/no-growth results as a function of pH and total carbonate concentration ($[HCO_3^-] + [CO_3^{2-}]$). Open circles indicate conditions at which no growth was observed; filled triangles indicate conditions at which growth occurred; no symbol (two horizontal lines) indicates indeterminate results. Error bars account for pH drift over the course of the 1.5 h incubation. Dashed curves approximately separate the regions of growth and no growth. The labeled bands indicate the ranges of published values for molluscan extrapallial fluid and natural seawater. Note that the range for extrapallial fluid, in which shell growth occurs biologically, spans the boundary between the growth and no-growth conditions.

biological mechanisms that control its formation are complex and only partially understood. Previous research (Wilbur, 1972; Weiner, 1986; Lowenstam and Weiner, 1989; Simkiss and Wilbur, 1989; Weiner and Addadi, 1991; Addadi and Weiner, 1992) suggests that shell mineralization commences with isolation of the site of mineralization from the external seawater environment by an insoluble matrix of macromolecules and the mantle tissue from which these molecules are secreted as an extension of the growing shell edge. The shell and the mantle epithelium enclose the extrapallial fluid, which is ionically enriched and pH-controlled by enzymatic pumping across the cell membranes of the mantle epithelium (Weiner and Traub, 1984; Weiner and Addadi, 1991). It has been suggested that insoluble matrix molecules play essential roles both in the control of crystal nucleation and by establishing compartments that limit the spaces in which the crystals grow (*e.g.*, Wilbur, 1972; Weiner, 1984; Nakahara, 1989). New aragonite crystals on the growth surface seem to be nucleated in pores of the organic matrix (Nakahara *et al.*, 1982), forming as small crystallites that grow to become the next nacreous layer (Wada, 1972). Crystal growth apparently also is controlled by several polyanionic proteins found associated with (and in some cases, occluded within) the mineral crystals; these proteins also have been suggested to act both in nucleation and in selective inhibition of crystal growth (Addadi and Weiner, 1985; Sikes and Wheeler, 1988; Addadi *et al.*, 1990; Weiner and Addadi, 1991; Morse *et al.*, 1993; Albeck *et al.*, 1993; Berman *et al.*, 1993).

The experiments reported here demonstrate that an exposed surface of mature nacre can continue to grow by purely inorganic means when the ion concentrations present in the extrapallial fluid favor the aragonite phase (primarily due to the presence of magnesium) and are supersaturated with respect to that form. This indicates that once the nucleation of the mineral phase has begun, the crystal can continue to grow without direct biological control. Therefore the requirements for nucleation, possibly including a template of acidic proteins (Aizenberg *et al.*, 1994; Morse *et al.*, 1993; Weiner *et al.*, 1983) or mineral bridges between the aragonite tablets (Manne *et al.*, 1994), can be independent of growth. Because the supersaturation levels required for overgrowth can be quite low, it is plausible that cells of the mantle could regulate growth simply by adjusting carbonate concentration and pH in the extrapallial fluid.

Although evidence for growth was decisive in most of the observed cases, quantification of the rates of mineral growth proved difficult since growth was not observed to occur uniformly over the experimental period. In some instances, growth occurred in the first few minutes of imaging after introducing a solution; in others, growth was not apparent until after the 1.5-h incubation. Unlike the case of the cleavage plane of geological calcite (Hillner *et al.*, 1993), on which growth occurs by quantifiable accretion of widely spaced steps, the aragonite tablet is much rougher and has a far greater step density. This high concentration of reactive sites may set up complex concentration gradients that affect the reaction rate in unpredictable ways.

It is interesting that the aragonitic overgrowth of nacre occurred in the form of needlelike extensions of the (001) surface, rather than as the layered growth characteristic of nacreous tablets in molluscan shells. The former is the common growth morphology of abiogenic aragonite and often results in extensive lateral intergrowth, producing fanlike aggregates of misaligned needles. Development of the highly coherent tablet morphology found in biogenic nacre, characterized by a high degree of orientation of the crystallographic *c* axes of the aragonite tablets, thus would require suppression of the tendency for disorder observed in the overgrowth process seen in our experiments. One possibility is that the highly anionic, soluble proteins (and possibly other macromolecules) found intimately associated with the aragonite crystals in molluscan nacre may prevent long-range incoherent intergrowth of the needles by specific interactions at the growing crystal surfaces (Addadi and Weiner, 1985). This would produce the coherent (001) surface and single crystal composition observed in mature nacre. In addition, the insoluble polymers of the matrix may help determine the final crystal form by creating a preformed microstructure that delimits the space in which the tablets grow (Wada, 1972; Nakahara, 1989). As neither the soluble acidic proteins nor empty sheaths of the insoluble matrix proteins were present in our experiments, growth along the *c* axis was persistently the fastest, as in abiogenic aragonite.

Acknowledgments

We thank Robert Petty (of the Marine Science Institute Analytical Laboratory, University of California, Santa Barbara) for performing the atomic absorption measurements; Monika Fritz, Angela Belcher, Charlotte Zaremba, and Deron Walters for useful discussions; and J. M. Didymus (School of Chemistry, University of Bath, UK) for kindly performing the calculations of supersaturation fractions. This work was supported by grants from the Materials Research Laboratory program of the National Science Foundation (DMR-9123048); the Molecular and Cellular Biosciences and Materials Research Divisions of the National Science Foundation (MCB-9202775 to G.D.S., D.E.M., and P.K.H.); the

Office of Naval Research (N00014-93-1-0584 to D.E.M., G.D.S., and P.K.H.); and a fellowship from AT&T (S. Manne).

Literature Cited

Addadi, L., and S. Weiner. 1985. Interactions between acidic proteins and crystals: stereochemical requirements in biomineralization. *Proc. Natl Acad Sci USA* **82:** 4110–4114.

Addadi, L., and S. Weiner. 1992. Control and design principles in biological mineralization. *Angew Chem Int Ed Engl* **31:** 153–169.

Addadi, L., A. Berman, J. Moradian-Oldak, and S. Weiner. 1990. Tuning of crystal nucleation and growth by proteins: molecular interactions at solid-liquid interfaces in biomineralization. *Croat Chem. Acta* **63:** 539–544

Aizenberg, J., S. Albeck, S. Weiner, and L. Addadi. 1994. Crystal-protein interactions studied by overgrowth of calcite on biogenic skeletal elements. *J Crystal Growth* **142:** 156–164.

Albeck, S., J. Aizenberg, L. Addadi, and S. Weiner. 1993. Interactions of various skeletal intracrystalline components with calcite crystals. *J Am. Chem Soc* **115:** 11691–11697.

Allen, M. J., N. V. Hud, M. Balooch, R. J. Tench, W. J. Siekhaus, and R. Balhorn. 1992. Tip-radius artifacts in AFM images of protamine-complexed DNA fibers. *Ultramicroscopy* **42–44:** 1095.

Berman, A., J. Hanson, L. Leiserowitz, T. F. Koetzle, S. Weiner, and L. Addadi. 1993. Biological control of crystal texture: a widespread strategy for adapting crystal properties to function. *Science* **259:** 776–777.

Binnig, G., C. F. Quate, and Ch. Gerber. 1986. Atomic Force Microscope. *Phys Rev. Lett* **56:** 930–933.

Cariolou, M. A., and D. E. Morse. 1988. Purification and characterization of calcium-binding conchiolin shell peptides from the mollusc, *Haliotis rufescens*, as a function of development. *J Comp Physiol B* **157:** 717–729.

Crenshaw, M. A. 1972. The inorganic composition of molluscan extrapallial fluid. *Biol Bull* **143:** 506–512.

Dove, P. M., and M. F. Hochella Jr. 1993. Calcite precipitation mechanisms and inhibition by orthophosphate: *in situ* observations by scanning force microscopy. *Geochim Cosmochim Acta* **57:** 705–714.

Friedbacher, G., P. K. Hansma, E. Ramli, and G. D. Stucky. 1991. Imaging powders with the atomic force microscope: from biominerals to commercial materials. *Science* **253:** 1261–1263.

Giles, R., S. Manne, C. M. Zaremba, A. Belcher, S. Mann, D. E. Morse, G. D. Stucky, and P. K. Hansma. 1993. Imaging single nacreous tablets with the atomic force microscope. *Materials Res Soc Proc.* **332:** (Boston, Fall 1993, in press).

Gratz, A. J., and P. E. Hillner. 1993. Poisoning of calcite growth viewed in the AFM. *J Crystal Growth* **129:** 789–793.

Gratz, A. J., P. E. Hillner, and P. K. Hansma. 1993. Step dynamics and spiral growth on calcite. *Geochim. Cosmochim Acta* **57:** 491–495.

Grütter, P., W. Zimmermann-Edling, and D. Brodbeck. 1992. Tip artifacts of microfabricated force sensors for atomic force microscopy. *Appl. Phys Lett* **60:** 2741–2743.

Hillner, P. E., A. J. Gratz, S. Manne, and P. K. Hansma. 1992. Atomic scale imaging of calcite growth and dissolution in real time. *Geology* **20:** 359–362.

Hillner, P. E., S. Manne, A. J. Gratz, and P. K. Hansma. 1993. Atomic force microscope: a new tool for imaging crystal growth processes. *Faraday Discuss Chem Soc* **95:** 191–197.

Hoh, J. H., and P. K. Hansma. 1992. Atomic Force Microscopy for high-resolution imaging in cell biology. *Trends Cell Biol.* **2:** 208–213.

Kasas, S., A. Berdal, and M. R. Celio. 1993. Tooth structure studied using the atomic force microscope. *Scanning Probe Microscopies II*, C. C. Williams, ed., *Proc. SPIE* **1855:** 17–25.

Kitano, Y., and D. W. Hood. 1962. Calcium carbonate crystal forms formed from seawater by inorganic processes. *J Oceanogr. Soc. JPN* **18:** 35–39.

Linder, A., J. Colchero, H.-J. Apell, O. Marti, and J. Mlynek. 1992. Scanning force microscopy of diatom shells. *Ultramicroscopy* **42–44:** 329–332.

Lowenstam, H. A., and S. Weiner. 1989. *On Biomineralization.* Oxford University Press, New York.

Manne, S., C. M. Zaremba, R. Giles, L. Huggins, D. A. Walters, A. Belcher, D. E. Morse, G. D. Stucky, J. M. Didymus, S. Mann, and P. K. Hansma. 1994. Atomic force microscopy of the nacreous layer in mollusc shells. *Proc. R. Soc. Lond. B* **256:** 17–23.

Morse, D. E., M. A. Cariolou, G. D. Stucky, C. M. Zaremba, and P. K. Hansma. 1993. Genetic coding in biomineralization of microlaminate composites. In *Biomolecular Materials*, C. Viney, S. T. Case, and J. H. Waite, eds. *Materials Res Soc. Proc.* **292:** 59–67.

Nakahara, H. 1989. Nacre formation in bivalve and gastropod molluscs. Pp. 343–350 in *Mechanisms and Phylogeny of Mineralization in Biological Systems*, S. Suga and H. Nakahara, eds. Springer-Verlag, New York.

Nakahara, H., G. Bevelander, and M. Kakei. 1982. Electron microscopic and amino acid studies on the outer and inner shell layers of *Haliotis rufescens*. *Venus* **41:** 33–46.

Pytkowicz, R. M. 1965. Rates of inorganic calcium carbonate nucleation. *J Geol* **73:** 196–199.

Rugar, D., and P. K. Hansma. 1990. Atomic Force Microscopy. *Physics Today* **43:** 23–30 (October).

Sabbides, T. G., and P. G. Koutsoukos. 1993. The crystallization of calcium carbonate in artificial seawater; role of the substrate. *J Crystal Growth* **133:** 13–22.

Sarid, D. 1991. *Scanning Force Microscopy: With Applications to Electric, Magnetic, and Atomic Forces.* Oxford University Press, New York.

Sikes, C. S., and A. P. Wheeler. 1988. Regulators of biomineralization. *Chemtech* **1988:** 620–626.

Simkiss, K., and K. M. Wilbur. 1989. *Biomineralization* Academic Press, New York.

Shellis, R. P. 1988. A microcomputer program to evaluate the saturation of complex solutions with respect to biominerals. *Cambios* **4:** 373–379.

Smith, F. G. W., ed. 1974. *CRC Handbook of Marine Science*, Vol. 1, p. 4. CRC Press, Cleveland, Ohio.

Tao, N. J., and S. M. Lindsay. 1992. Measuring the microelastic properties of biological material. *Biophys J* **63:** 1165–1169.

Towe, K. M. 1972. Invertebrate shell structure and the organic matrix concept. *Biomineralisation* **4:** 1–14.

Wada, K. 1961. Crystal growth of molluscan shells. *Bull Natl. Pearl Res Lab JPN* **7:** 703–828.

Wada, K. 1972. Nucleation and growth of aragonite crystals in the nacre of some bivalve molluscs. *Biomineralisation* **6:** 141–159.

Wada, K., and T. Fujinuki. 1976. Biomineralization in bivalve molluscs with emphasis on the chemical composition of the extrapallial fluid. Pp. 175–190 in *The Mechanisms of Mineralization in the Invertebrates and Plants*, N. Watabe and K. M. Wilbur, eds. University of South Carolina Press, Columbia, South Carolina.

Watabe, N. 1981. Crystal growth of calcium carbonate in the invertebrates. *Prog. Crystal Growth Charact.* **4:** 99–147.

Weiner, S. 1984. Organization of organic matrix components in mineralized tissues. *Am. Zool.* **24:** 945–952.

Weiner, S. 1986. Organization of extracellularly mineralized tissues: a comparative study of biological crystal growth. *CRC Crit. Rev. Biochem.* **20:** 365–408.

Weiner, S., and L. Addadi. 1991. Acidic macromolecules of mineralized tissues: the controllers of crystal formation. *Trends Biochem. Sci.* **16:** 252–256.

Weiner, S., and W. Traub. 1980. X-ray diffraction study of the insoluble organic matrix of mollusk shells. *FEBS Lett.* **111:** 311–316.

Weiner, S., and W. Traub. 1984. Macromolecules in mollusc shells and their functions in biomineralization. *Phil. Trans. R. Soc. Lond B* **304:** 425–434.

Weiner, S., Y. Talmon, and W. Traub. 1983. Electron diffraction of mollusc shell organic matrices and their relationship to the mineral phase. *Int. J. Biol. Macromol.* **5:** 325–328.

Wierzbicki, A., C. S. Sikes, J. D. Madura, and B. Drake. 1993. Atomic force microscopy and molecular modeling of protein and peptide binding to calcite. *Calcif. Tiss. Int.* **54:** 133–141.

Wilbur, K. M. 1972. Shell formation in mollusks. Pp. 103–145 in *Chemical Zoology, Vol. 6: Mollusca,* M. Florkin and B. T. Scheer, eds. Academic Press, New York.

Wilbur, K. M., and A. M. Bernhardt. 1984. Effects of amino acids, magnesium, and molluscan extrapallial fluid on crystallization of calcium carbonate: *in vitro* experiments. *Biol. Bull.* **166:** 251–259.

Wise, S. W. 1970. Microarchitecture and mode of formation of nacre (mother-of-pearl) in pelecypods, gastropods, and cephalopods. *Eclogae Geol. Helv.* **63:** 775–797.